

An optical lattice with single lattice site optical control for quantum engineering

R Scheunemann[†], F S Cataliotti^{†§}, T W Hänsch^{†‡} and M Weitz^{†‡}

[†] Max-Planck-Institut für Quantenoptik, Hans-Kopfermann-Str. 1, 85748 Garching, Germany

[‡] Sektion Physik der Universität München, Schellingsstr. 4, 80799 München, Germany

Received 5 January 2000, in final form 5 July 2000

Abstract. We resolve and address atoms in single sites of an optical lattice with a period of $5.3 \mu\text{m}$ created by a retroreflected, focused CO_2 laser beam. In this one-dimensional lattice, the Lamb–Dicke limit can be fulfilled in all three spatial dimensions. Because of the negligible decoherence rate from spontaneous photon scattering such a lattice offers unique possibilities for the study of quantum phenomena in a controllable environment.

Keywords: Quantum transport, optical lattice, laser cooling, dipole trap, quantum logic, quantum computing, atom trap

(Some figures in this article appear in colour in the electronic version; see www.iop.org)

1. Introduction

In recent years, the principal limitation of near-resonant optical lattices, i.e. photon scattering, has been circumvented by the use of far-detuned dipole traps (see, for example, [1]). Typically, in these systems it is possible to achieve coherence times of the order of seconds while maintaining the freedom to choose an almost arbitrary form of the trapping potential. A very promising extension of such an optical lattice can be realized using a CO_2 laser beam at $10.6 \mu\text{m}$, focused to create a trap that can hold virtually any atomic or molecular species. In such a trap the scattering rates are of the order of photons per hour, while the vibrational frequencies can be made very high in standing wave configurations [2]. This allows the search for permanent electric dipole moments in atoms, the possible realization of quantum degeneracy via optical means alone or the study of trapped cold molecules [3]. In the standing wave configuration created by simply retroreflecting the CO_2 laser beam back on itself, the atomic microtraps are spaced by $5.3 \mu\text{m}$. Despite this large spacing of roughly seven times the wavelength of the rubidium D2 line, the Lamb–Dicke regime, corresponding to a spacing of vibrational levels above the photon recoil energy, is readily reached in such a lattice [2]. This suggests that the trapped atoms could be cooled to the vibrational ground state by sideband cooling, as demonstrated first in pioneering experiments with single ions in Paul traps [4]. With neutral atoms, sideband cooling in optical lattices has been achieved more recently [5]. Due to their spatial periodicity, optical lattices can serve as model systems to study quantum effects in

solid state physics, as for example demonstrated by the observation of Bloch oscillations [6] and Wannier–Stark ladders [7]. More generally, atoms in the ground state of an optical lattice provide an intriguing system to explore quantum state control (see, for example, [8]). Traditionally, optical lattices have been investigated by monitoring their (quantized) vibrational frequencies (see, for example, [9]), and the solid state properties observed more recently in such lattices were also observed in the frequency domain.

We will focus here on the possibility offered by the large lattice spacing of a CO_2 laser optical lattice to resolve and control atoms in single lattice sites. The use of a spacing clearly above the wavelength of resonant light provides a natural method for lattice investigations in the spatial domain. In future, this type of lattice should allow novel possibilities for quantum state control. Upon cooling the atoms to the lowest vibrational level, it should, for example, be possible by adiabatic lowering of the potential to create a band structure. The possibility of manipulating single sites could then allow one to study the propagation of density variations. Along related lines, quantum tunnelling between sites of this lattice could be directly observed. Alternative research prospects include quantum logic operation [10, 11] and the possible realization of Bose–Einstein condensation (BEC) by optical means only [12].

In section 2 of this paper we briefly review the most important properties of a CO_2 laser optical lattice while in section 3 we sketch our experimental setup. Section 4 is dedicated to the issue of loading the far-off resonance optical lattice from a magneto-optical trap (MOT) with particular attention to the attainable temperatures and densities and to the limitations posed by the differential ac-Stark shift in

[§] On leave from: Dipartimento di Fisica, Università di Firenze, I-50125, Firenze, Italy.

ground and excited states. In section 5 we describe how it is possible to resolve and manipulate single lattice sites. The last section outlines some future prospects of this research, mainly focusing on further cooling inside the lattice.

2. Trapping potential for atoms

In optical lattices, the trapping potential is provided by the interaction of the induced atomic dipole with the focused laser field. In our work, the potential is generated by the radiation of a CO₂ laser operating near 10.6 μm . The laser frequency is more than one order of magnitude lower than any dipole transition starting from the ground or first excited states of rubidium. The induced potential is thus well approximated by the static Stark shift $U = -1/2\alpha_s|E|^2$, where α_s is the static atomic polarizability and $|E|$ is the amplitude of the light field. If the trap is formed by the interference of two laser beams of equal power P and polarizations e_1 and e_2 respectively, focused to a waist s_0 , the resulting potential for the rubidium 5S ground state is

$$V(r, z) = -4V_{\max}(z) \times \exp\left[-\frac{2r^2}{s(z)^2}\right] \left[1 - \cos^2\left(\frac{2\pi z}{\lambda}\right) e_1 \cdot e_2\right] \quad (1)$$

where $V_{\max}(z) = \alpha_s P/[c\epsilon_0\pi s(z)^2]$ and $s(z) = s_0\sqrt{1 + (z/z_R)^2}$, with $z_R = \pi s_0^2/\lambda$ as the Rayleigh length. This expression is valid to order $(\Delta_{\text{FS}}/\Delta)$ (with Δ_{FS} as the fine structure splitting and Δ as the CO₂ laser detuning from the centroid of the 5P states) for every sublevel of the ground state. During the laser cooling process, atoms are being excited from the ground state into the 5P_{3/2} state, from which they spontaneously decay back into the ground state. The potential for P states depends both on the laser polarization and the particular sublevel. One finds that the ac-Stark shift for all sublevels of the 5P_{3/2} excited state is the same to within roughly 13%. The excited state potential has the same sign as the ground state potential, i.e. it attracts atoms in high-intensity regions. The Stark shift of the 5P centroid is, however, a factor of 2.89 larger than that of the 5S ground state.

The trapping potential leads to a confinement of cold atoms in the antinodes of the standing wave spaced by $\lambda/2$ or 5.3 μm . If $V_{\max}(z)$ is large compared with the atomic thermal energy, the potential in each microtrap can be approximated by a harmonic oscillator potential $V_j(r, z) = (m/2)\omega_{j,r}^2 r^2 + (m/2)\omega_{j,z}^2 z^2$. The vibrational frequencies are $\omega_{j,r} = \omega_{\max}\sqrt{1 - 4(z_j/z_R)^2}$ and $\omega_{j,z} = (\pi s_0/\lambda)\omega_{\max}\sqrt{1 - 2(z_j/z_R)}$, where we have defined $\omega_{\max} = 4\sqrt{V_{\max}(0)/m}/\pi s_0$. For ⁸⁵Rb atoms confined in a 14 W CO₂ laser standing wave focused to a waist of 35 μm , the maximum potential depth is 2.1 mK and the expected vibrational frequencies are 5.7 kHz radially and 59 kHz longitudinally. This kind of lattice can be loaded with atoms from a MOT, where the temperatures are of the order of a few μK . Furthermore, the vibrational splitting exceeds the atomic recoil energy $\hbar\omega_{\text{rec}} = h^2k^2/2m$ for photons near the D1 transition $\lambda = 794$ nm, which corresponds to a frequency $\omega_{\text{rec}} = 2\pi \cdot 3.8$ kHz, i.e. we can reach the Lamb–Dicke regime clearly in the axial and just in the radial dimension in this one-dimensional lattice. With higher laser power or smaller

optical focus diameters a further increase of the vibrational frequencies could be achieved. One main advantage of the use of a CO₂ laser beam at 10.6 μm is the almost complete suppression of trap light scattering. The Rayleigh scattering rate is given by the expression

$$\Gamma_S = \frac{16r_0^2 P}{3\hbar\omega_0^2} \left(\frac{m_e\alpha_s}{e^2}\right)^2 \omega_{\text{CO}_2}^3 \quad (2)$$

where r_0 is the classical electron radius, m_e is the electron mass and ω_{CO_2} is the optical frequency of the CO₂ laser light. Spontaneous Raman scattering is suppressed by an additional factor of $(\Delta_{\text{FS}}\omega_{\text{CO}_2}/\omega_{\text{D1}})^2$, where ω_{D1} denotes the frequency of the atomic D1 line [3]. In the numerical example described above, the Rayleigh rate is of the order of 5 mHz, allowing for trapping times comparable to magnetic traps [13]. Let us point out that, in addition to the suppression of scattering of photons from the trapping light, the reabsorption of photons from the cooling light scattered by atoms from neighbouring lattice sites is also suppressed in our one-dimensional lattice arrangement, as only a few fluorescence photons are emitted precisely along the lattice axis. The reabsorption probability decreases with temperature, as lower temperatures result in a better transverse localization of the atoms, yielding a smaller solid angle of an atomic microcloud seen from neighbouring trap sites.

3. Experiment setup

Our experimental setup is shown in figure 1. A combination of an ion pump and titanium sublimation pump yields a background pressure in the vacuum chamber below 1×10^{-9} mbar. A resistively heated alkali metal dispenser provides a compact and controllable source of thermal rubidium atoms [14]. A single-mode CO₂ laser generates an output power up to 50 W near 10.6 μm . Its infrared beam passes an acousto-optic modulator (AOM), which is used both for optical isolation and to control the beam intensity. Two adjustable ZnSe lenses inside the vacuum chamber and a retroreflecting mirror are used to form a standing wave with a beam waist of typically 35 μm .

Atoms of the isotope ⁸⁵Rb are collected and pre-cooled in a MOT. A free-running diode laser injection locked to a second, grating-stabilized diode provides the cooling light detuned to the red side of the 5S_{1/2}, $F = 3$ to 5P_{3/2}, $F = 4$ cycling transition. The atoms are repumped into the cooling cycle by a grating-stabilized third laser locked to the 5S_{1/2}, $F = 2$ to 5P_{3/2}, $F = 3$ transition. We control the intensity of the cooling and repumping beams with AOMs. Both cooling and trapping beams are focused through pinholes to clean the mode and then enlarged to a diameter of 20 mm. We can also mechanically shut off all MOT beams.

A Questar long-distance microscope QM100 placed 10 cm away from the trap centre outside the vacuum system has been used to image the trapped atoms onto an intensified CCD (ICCD) camera. This results in a magnification of the lattice by a factor of eight. In this configuration we could take pictures of the expansion of the atoms released from the optical lattice. This time-of-flight method was used to locally measure the atomic temperatures along the

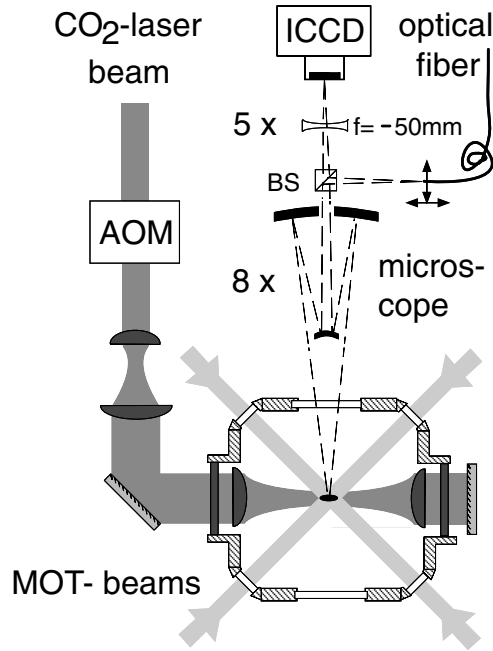


Figure 1. Schematic illustration of the experimental apparatus.

radial direction. To image the optical lattice, we inserted an additional biconcave lens of $f = -50$ mm focal length between the microscope and camera. This results in an enlargement of the image by an additional factor of five. With this total magnification of 40, the rescaled pixel size is $0.6 \mu\text{m}$ and the field of view is $346 \times 230 \mu\text{m}^2$. Light from an additional laser resonant with the $5S_{1/2}$, $F = 3$ to $5P_{3/2}$, $F = 4$ cycling transition has been sent through the core of an optical fibre and is imaged via a beamsplitter through the microscope onto the sample. The optical setup here represents that of a confocal microscope and allows the illumination of only a small area of the lattice.

4. Loading the lattice

Our experimental sequence starts by loading the MOT for 3 s. The cooling laser is operated with a detuning of 2 linewidths ($\Gamma = 2\pi \cdot 6$ MHz) red of the cooling transition. The total power in this beam is 20 mW. During this phase the repumping laser is operated with a total power of around 5 mW. At the end of this phase, we collect around 1×10^7 ^{85}Rb atoms with a temperature of $30(5) \mu\text{K}$ and a density of 2×10^9 atoms cm^{-3} . We then instantaneously switch on the lattice potential while applying a dark MOT phase. In this phase, the repumping laser intensity is reduced by a factor of ten and the detuning of the cooling laser is increased to -13Γ . At the end of this phase, all the resonant light fields and the MOT magnetic quadrupole field are switched off. The atoms are now trapped in the lower hyperfine ground state and the atomic cloud is then observed by pulsing on the MOT beams and imaging the fluorescence onto both a calibrated photodiode and an ICCD camera. We determined the temperature of the atoms by switching off the trapping potential and observing the ballistic expansion of the cloud. Figure 2(a) shows the measured

number of atoms and their peak density as a function of the CO₂ laser power at a beam waist s_0 of $50 \mu\text{m}$. Both the number of captured atoms and the peak density increase with the laser power, but tend to saturate. At the maximum available power of 37 W we measure a loading efficiency of 15% and a peak density $n_{\text{peak}} = N / (2\pi)^{3/2} \sigma_x \sigma_y \sigma_z$ of $3.2(5) \times 10^{13}$ atoms cm^{-3} , where $2\sigma_i$ is the spatial extension in the i -direction, corresponding to a density increase of more than four orders of magnitude with respect to the MOT. On the other hand, the temperature of the trapped atoms increases with the trapping laser power, as shown in figure 2(b). While for small trapping beam intensities we reach a minimum temperature of $18(5) \mu\text{K}$, for larger intensities the atomic temperature increases up to approximately the Doppler limit. Figure 2(b) also shows the product $\eta = n_{\text{peak}} \lambda_{\text{dB}}^3$, where λ_{dB} denotes the thermal deBroglie wavelength, which drops from $1/300$ to 10^{-4} when increasing the CO₂ laser power from 5 to 35 W. Note, that the value for η must still be divided by the number of populated Zeeman levels to yield the true phase space density. One could, however, argue that the used polarization gradient cooling locally pumps the atoms into one (or few) Zeeman sublevels. We attribute the intensity-dependent temperature to the differential ac-Stark shift of the ground and excited states in the trapping laser field. As mentioned in section 3, the ac-Stark shift of the $5P_{3/2}$ states is more than twice that of the ground state. This creates a position-dependent detuning, which becomes significant for larger trapping laser intensities. If the effective detuning is always negative (low-power regime), we have a higher viscosity in the centre of the dipole trap and the atoms are loaded and cooled in the trap. On the other hand, if for higher laser powers the ac-Stark shift is so large that the effective detuning changes sign and becomes blue in the trap centre we will have heating in the trap centre and a reduced loading efficiency. It is not possible to increase the red detuning of the cooling laser indefinitely because of the presence of other hyperfine levels. In a simplified picture we can argue that, for high trapping powers, the excited state hyperfine structure is no longer resolved across the trap region and this results in higher temperatures. This reduces the efficiency of polarization gradient cooling.

We have followed the method outlined in [15] to derive the force acting on an atom for counter-propagating laser beams with opposite circular polarizations in the one-dimensional case. The effect of the trapping potential has been included as a position-dependent detuning, which is justified since the trap oscillation frequencies are much smaller than the optical pumping times. We have accounted for all the magnetic sublevels within the D2 manifold. The result of such a simulation confirms the above qualitative discussion.

The reduced cooling and loading efficiency for higher laser powers is very clearly visible in figure 3, where it is shown that at high powers a smaller fraction of atoms is loaded in the centre of the lattice. The measured atomic temperature is not uniform along the lattice axis. We find higher atomic temperatures and densities in the central region. These are the values reported in figure 2 and discussed in the text.

We have also measured the dependence of the lattice temperature on the cooling laser detuning during the dark

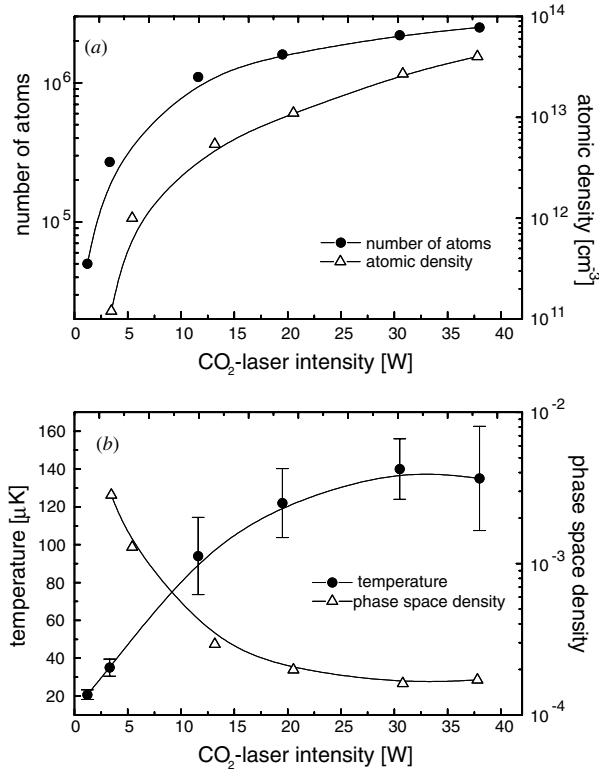


Figure 2. (a) Number of atoms and density as a function of CO₂ laser power. (b) Temperature and phase space density as a function of CO₂ laser power.

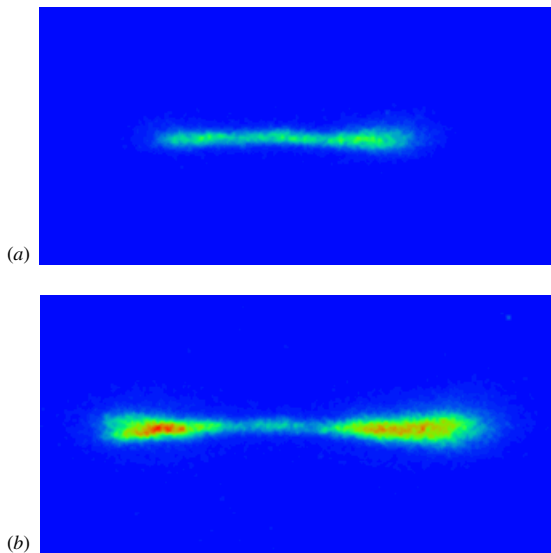


Figure 3. (a) Low-magnification image of rubidium atoms trapped in the one-dimensional optical lattice. In the low-power regime atoms are loaded in the trap centre (P_{CO₂} = 3.5 W, s₀ = 35 μm). (b) As (a), but in the high-power regime (P_{CO₂} = 20 W, s₀ = 35 μm). Very few atoms can be loaded in the trap centre due to the large differential ac-Stark shift.

MOT phase. For low CO₂ laser powers, the temperature shows a minimum at a detuning slightly above the 5S_{1/2}, F = 3 to 5P_{3/2}, F = 3 transition. We attribute this to the reduction of light scattering achieved in a blue optical molasses, which results in a reduced lattice temperature [16]. For higher laser

powers no such behaviour is observed.

We have measured vibrational frequencies by parametrically exciting the atoms as described previously [2]. Briefly, the CO₂ laser beam intensity is modulated by the AOM, and significant vibrational excitation occurs if the modulation frequency equals twice a trap vibrational frequency. The induced trap loss, resulting in a reduced fluorescence, is recorded with the intensified CCD camera to allow a spatially resolved fluorescence measurement. Since the oscillation frequencies depend strongly on the position of the microtraps along the symmetry axis of the lattice, this is of importance here. With typical parameters of 14 W of CO₂ laser power and a 35 μm waist we measure oscillation frequencies in the central trap region of ν_z = 54(5) kHz in the axial and ν_r = 4.2(5) kHz in the radial direction, which is in reasonable agreement with the calculation of section 2. The Lamb-Dicke limit, corresponding to an oscillation frequency above ν_{rec} = 3.8 kHz, is therefore fulfilled in all three spatial dimensions.

For a future sideband cooling of the atoms it seems best to load the lattice at small CO₂ laser intensity which results in the highest phase space densities, and then adiabatically ramp up to full laser intensity to achieve high vibrational frequencies.

We have observed a lifetime of 3.4 s limited by collisions with the thermal rubidium background gas. In the future, by pulsing our atomic source, it should be possible to obtain lifetimes as long as 20 s limited only by the residual pressure in our vacuum system [13].

5. Resolving the lattice

To image the optical lattice, the power of the CO₂ laser beam was reduced to 4 W to achieve lower temperatures. We loaded the lattice as described previously, and, after trapping the atoms for 100 ms in the lattice, the CO₂ laser beam was switched off. The MOT lasers were then pulsed on for 20 μs while accumulating the atomic fluorescence with the ICCD camera. We have chosen the detuning of the cooling laser to be resonant with the cycling transition and also added repumping light. Figure 4(a) shows the image of 50 accumulated recordings after subtraction of a constant background due to spurious scattered light and dark counts. One observes the localization of atoms in periodically spaced pancake-like microtraps of 5.3 μm period, each of these sites now containing up to 4 × 10³ atoms. From this plot, we can evaluate a contrast defined as $C = (I_{\max} - I_{\min}) / (I_{\max} + I_{\min})$ of 32(5)%, which gives a quantitative measure for resolving the lattice. From the measured vibrational frequencies and the atomic temperature ($T = 52 \mu\text{K}$ for this data set), we can estimate the actual size of the atomic micro-clouds when assuming $k_{\text{B}}T/2 = 2\pi^2 m v_i^2 \sigma_i^2$ for atoms in a harmonic potential. The calculated radial width $\sigma_r^{\text{theo}} = 5.2 \mu\text{m}$ is in reasonable agreement with the measured value of $\sigma_r = 6.8(7) \mu\text{m}$ HWHM assuming a Gaussian density distribution in the trap. The calculated axial width of the micro-clouds is $\sigma_z^{\text{theo}} = 0.4 \mu\text{m}$, which results in an expected perfect contrast for the lattice cross section as this width is much smaller than the lattice periodicity. We attribute the measured contrast to be mainly limited by the finite resolution of our

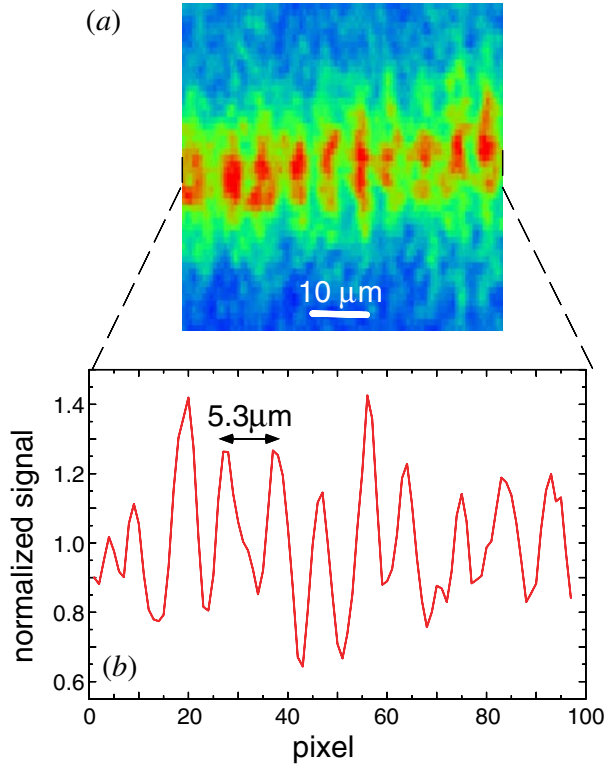


Figure 4. (a) Magnified image of rubidium atoms trapped in a one-dimensional optical lattice with a period of $5.3 \mu\text{m}$. The axis of the infrared CO_2 laser beam is oriented horizontally. (b) Cross section of this image obtained by integrating the measured atomic fluorescence perpendicular to the trapping beam axis.

imaging system and derive a value for the resolution by modelling the image by convoluting the expected picture with a Gaussian broadening of variable width. From a fit of this simple model to the cross section, we can estimate the spatial resolution of our imaging system to be $1.9 \mu\text{m}$. This measurement shows that it is possible to distinguish atoms in neighbouring lattice sites. This would eventually allow us to read out the information of individual quantum bits stored in the antinodes of this one-dimensional optical lattice. At present, we are using an optical imaging system optimized for the visible spectral region. The optical resolution could be further improved by using a system optimized for the atomic fluorescence wavelength of 780 nm , i.e. the rubidium D2 line. Alternatively, one could use shorter wavelength transitions for the fluorescence imaging, e.g. the $5\text{S}-6\text{P}$ line of the rubidium atom near 420 nm .

Figure 5(a) shows the image of the lattice of ^{85}Rb atoms illuminated by the MOT beams similarly as already described. Here the CO_2 trapping laser was left on during the entire cycle. This allowed illumination times as long as $100 \mu\text{s}$. In the absence of the trapping field the contrast of the images vanishes within $30 \mu\text{s}$ due to the thermal expansion of the cloud. For this measurement we chose the detuning of the cooling beams to be resonant with the $5\text{S}_{1/2}, F = 3$ to $5\text{P}_{3/2}, F = 4$ transition at the bottom of the central potential wells. Figure 5(b) shows an image taken by illuminating a single trapping site for a period of $100 \mu\text{s}$ with around $10 \mu\text{W}$ of light resonant with the $5\text{S}_{1/2}, F = 3$ to $5\text{P}_{3/2}, F = 4$

cycling transition at the bottom of the trap. This light was sent through the fibre and focused onto a single lattice site by the optical microscope. The MOT repumping beams were also switched on during this period. The exposure shows atoms localized in one distinct potential well of the standing wave, with the neighbouring lattice sites suppressed by a factor of approximately 2.3. Note that the rest of the lattice is still filled, but is not visible here. This shows that in principle it is possible to address single qubits in an optical lattice. In order to investigate whether the neighbouring wells were being perturbed by the focused laser beam, the following procedure was used. After loading the atoms into the trap, we applied a $10 \mu\text{s}$ long pulse of light through the fibre with the same frequency, but with 20 times higher intensity. Again, the MOT repumping beams were used to provide the necessary repumping light. Figure 5(c) shows the image of the lattice after interaction with such a pulse using the two MOT beams for exposure of the picture. The population of a single lattice site has been almost completely removed, while atoms in neighbouring sites are affected much less by the short pulse. We estimate the $1/e$ -diameter of the imaged focus in figure 5(c) to be $9 \mu\text{m}$, which is above the lattice spacing. We attribute this fact to nonlinearities in the removing process. The atoms had to be illuminated by a relatively intense pulse of resonant light to also remove the tightly trapped atoms from a specific lattice site. Atoms in neighbouring sites that are less strongly bound can on the other hand quite easily be removed by the ‘wings’ of the imaged focus. In a future application of the addressing laser to perform single qubit operation, much lower intensities are necessary and therefore the interaction with atoms sitting in neighbouring sites can be further suppressed. Nevertheless, improvement of our imaging system certainly remains an important experimental issue for future work. By varying the position of the optical fibre along the axial direction of the lattice we could address different lattice sites within our optical field of view, which comprises around 50 lattice sites.

6. Future prospects

We are currently setting up an experiment to study Raman sideband cooling [5] in our optical lattice. The application of one-dimensional sideband cooling might already be sufficient to reach a significant population in the vibrational ground state of the microtraps. Indeed, due to the high atomic densities peculiar to our lattice the elastic collision rate should be sufficiently high to allow sympathetic cooling of the other dimensions. Alternatively, one could certainly proceed towards direct Raman cooling of all three spatial dimensions. As mentioned in section 2, our one-dimensional arrangement minimizes heating due to reabsorption of scattered photons. If the cooling process were to work all the way to the ground state, we could end up producing an array of independent micro-condensates in a completely new regime given the high vibrational frequencies obtained in our trapping potential.

Another possibility offered by our system would be to reduce the lattice potential while keeping the atoms inside the dipole trap. This would create a band structure similar to that described in [17]. If the potential were reduced adiabatically after cooling the atoms to the vibrational ground state, this

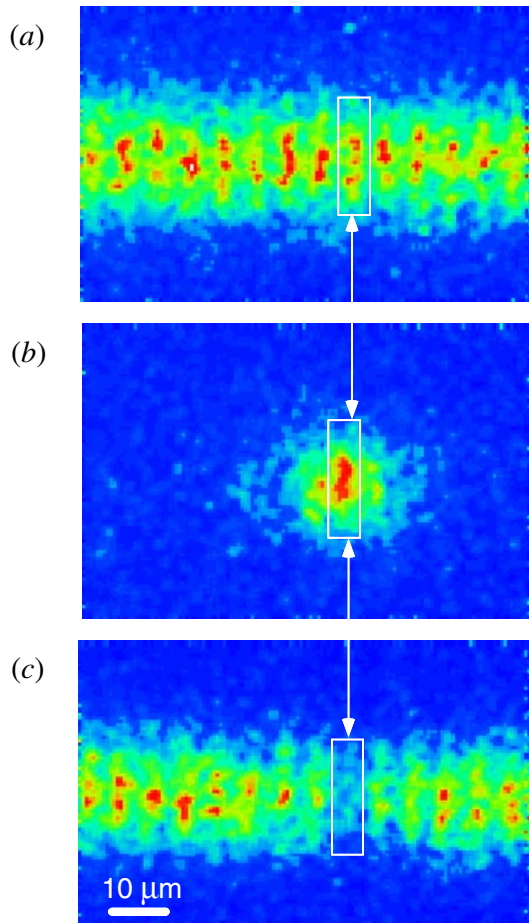


Figure 5. Images of the lattice after the following manipulations. (a) No manipulation of the atoms in the microtraps. (b) Only atoms from a single lattice site are illuminated during the exposure with a focused laser beam. (c) Image of the lattice after removing atoms in one lattice site before the exposure.

system would provide a unique system for the preparation of non-classical states of motion [18] and the study of mean-field effects in a totally controlled fashion. The possibility to spatially resolve the single lattice sites would be maintained, giving an important advantage with respect to conventional near-resonant lattices.

We also plan to explore the possibility of performing quantum logic operations with this far-detuned optical lattice [11]. To avoid rapid decoherence, the atoms must also be cooled to the vibrational ground state of the lattice. A coupling of different atoms should be possible, for example via controlled, cold collisions [19, 20].

To conclude, we have optically resolved an optical lattice based on the infrared radiation of a CO₂ laser operating near

10.6 μm . This type of optical lattice has exciting prospects in the broad field of quantum state engineering and the study of entanglement. In addition, our one-dimensional geometry minimizes reabsorption of photons emitted spontaneously when applying near-resonant cooling light. This could allow for the possibility of reaching BEC by optical cooling alone.

Acknowledgments

This work is supported in part by the Deutsche Forschungsgemeinschaft and within an EC Science contract.

References

- [1] Grimm R, Weidemüller M and Ovchinnikov Y B 2000 *Adv. At. Mol. Opt. Phys.* **42** 95
- [2] Friebe S, D'Andrea C, Walz J, Weitz M and Hänsch T W 1998 *Phys. Rev. A* **57** R20
- [3] Takekoshi T and Knize R J 1996 *Opt. Lett.* **21** 77
- Takekoshi T, Yeh J R and Knize R J 1995 *Opt. Commun.* **114** 421
- [4] Diedrich F, Bergquist J, Itano W and Wineland D 1989 *Phys. Rev. Lett.* **62** 403
- [5] Hamann S, Haycock D, Klose G, Pax D, Deutsch I and Jessen P 1998 *Phys. Rev. Lett.* **80** 4149
- Perrin H, Kuhn A, Bouchoule I and Salomon C 1998 *Europhys. Lett.* **42** 395
- Vuletic V, Chin C, Kerman A and Chu S 1999 *Phys. Rev. Lett.* **81** 5768
- Vuletic V, Chin C, Kerman A and Chu S 2000 *Phys. Rev. Lett.* **84** 439
- [6] Ben Dahan M, Peik E, Reichel J, Castin Y and Salomon C 1996 *Phys. Rev. Lett.* **76** 4508
- [7] Wilkinson S, Bharucha C, Madison K, Niu Q and Raizen M 1996 *Phys. Rev. Lett.* **76** 4512
- [8] 1997 Special issue on quantum state preparation and measurement *J. Mod. Opt.* **44** 2021ff
- [9] Jessen P S and Deutsch I H 1996 *Adv. At. Mol. Opt. Phys.* **37** 95
- [10] Briegel H-J, Calarco T, Jaksch D, Cirac J I and Zoller P 2000 *J. Mod. Opt.* **47** 415
- [11] Scheunemann R, Cataliotti F S, Hänsch T W and Weitz M *Phys. Rev. A* at press
- [12] Santos L, Lewenstein M, Cirac J I and Castin Y 1998 *Preprint quant-ph/9812025*
- [13] O'Hara K, Granada S, Gehm M, Sarad T, Bal S, Freed C and Thomas J 1999 *Phys. Rev. Lett.* **82** 4204
- [14] Fortagh J, Grossmann A, Hänsch T W and Zimmermann C 1998 *J. Appl. Phys.* **84** 6499
- [15] Bambini A and Agresti A 1997 *Phys. Rev. A* **56** 3040
- [16] Friebe S, Scheunemann R, Walz J, Hänsch T W and Weitz M 1998 *Appl. Phys. B* **67** 699
- [17] Steel M and Zhang W 1998 *Preprint cond-mat/9810284*
- [18] Moringa M, Bouchoule I, Karam J-C and Salomon C 1999 *Phys. Rev. Lett.* **83** 4037
- [19] Brennen G, Caves C, Jessen P and Deutsch I 1999 *Phys. Rev. Lett.* **82** 1060
- [20] Jaksch D, Briegel H-J, Cirac J I, Gardiner C W and Zoller P 1999 *Phys. Rev. Lett.* **82** 1975